Springer

KSME

Journal of Mechanical Science and Technology 32 (12) (2018) 5845~5853
www.springerlink.com/content/1738-494x(Print)/1976-3824(Online)
DOI 10.1007/s12206-018-1133-5

Analysis of geometrical characteristics of CNT-Al composite using molecular dynamics and the modified rule of mixture (MROM) †

Dong Mun Park[1], Jun Hwan Kim[1], Seung Jun Lee[2] and Gil Ho Yoon[1,*]

[1]*School of Mechanical Engineering, Hanyang University, Seoul 133-791, Korea*
[2]*School of Mechanical, Robotics, and Energy Engineering, Dongguk University, Seoul 100-715, Korea*

(Manuscript Received April 19, 2018; Revised August 24, 2018; Accepted September 3, 2018)

Abstract

This research presents molecular dynamics (MD) simulations to characterize the tensile behaviors of aluminum (Al) composites reinforced with carbon nanotubes (CNTs). The positions, alignments and condensations of CNT inside aluminum composites are stochastic in real and they influence the tensile behaviors of the composites. Thus, it is important to quantize the strengths of the CNT-Al composites depending on the configurations of CNTs. For this, the angles of the CNTs are varied inside an aluminum composite to estimate the yield strengths of the composites using MD simulation. Compared with the strength of pure Al composite, the Young's modulus of an aluminum composite increases about 20 GPa from 71.52 GPa to 92 GPa (Chiral vector (6,6), 0 degrees). However, with inclined carbon nanotubes, the strength is deteriorated due to the interface slip and the necking of Al block. Some deteriorations of yield stress and yield strain are observed due to premature failure of the CNT–Al composite due to local buckling. The present study also finds out that the modified rule of mixture (MROM) can be used to characterize the effect of geometrical characteristics of CNT-Al composite.

Keywords: Modified rule of mixture (MROM); Carbon nanotubes; Metal-matrix composites (MMCs); Modelling/simulations; Stress/strain measurements

1. Introduction

After the development of carbon nanotube with novel material properties, it has been used as an attractive reinforcing material for composites [1-13]. Many relevant experimental and computational researches to quantitate the material properties such as Young's modulus, Yield strength and fracture strength have been conducted [1-4, 7, 9, 11, 12, 14]. Furthermore, CNTs reinforced composites were used for polymer, ceramic and metal matrix for the sake of structural applications. Particularly aluminum (Al) has been used as basic composite material due to its good mechanical properties. To maintain its good mechanical properties in composite applications of CNTs, it is vital to uniformly disperse CNTs in metal or polymer as the material properties are strongly dependent on its uniform dispersion. To disperse CNTs uniformly, there are many researches for manufacturing techniques [9, 15-19]. By dispersing CNTs uniformly in Al, it has been reported that the mechanical properties can be greatly enhanced. In Ref. [18], the enhancements of tensile strength, Young's modulus and elongation of Al composites have been proved experimentally with differential scanning calorimetric, X-ray diffraction, field emission scanning electron microscopy and transmission electron microscopy. It is impressing that with 1 % inclusions of CNTs, the tensile strength and Young's modulus are improved to 521.7 MPa and to 102.2 GPa [9], respectively. The hardness is also increased with a vertically aligned array of CNTs with Al. Due to its vertical alignment, the material properties become anisotropic. In Refs. [8, 19-22], it was reported that the dispersion characteristics of CNTs is one of the important factors for material properties in CNT composites. Furthermore with the calibration using experiment results, several computational methods have been used to compute the mechanical behavior of nanocomposites [2, 8, 18, 23].

For computational simulations in nanoscale, there are the two major techniques: ab initio methods and molecular dynamics (MD) simulation. The ab initio method based on the quantum chemistry tries to solve of electronic Schrödinger equation in order to find out electron densities, energies and other properties. However, there is a disadvantage that the ab initio method takes a long time to simulate. Therefore, this research uses molecular dynamics simulation method which is less accurate than ab initio method but has an advantage in computational cost and useful to understand molecular failure mechanisms and to analyze mechanical properties of composite material. Xiao and Hou [13] employed the domain cou-

*Corresponding author. Tel.: +82 2 2220 0451
E-mail address: ghy@hanyang.ac.kr, gilho.yoon@gmail.com
† Recommended by Associate Editor Seong-Chan Jun

pling method to study the elastic modulus and fracture strength of CNT-based aluminum composites. In their simulation, carbon nanotubes and their surrounding atoms are modeled in the framework of MD simulation and the long range interactions are treated in connection to finite element procedure. Although all types of carbon nanotubes can enhance the strength of nanocomposites, multi-walled carbon nanotubes play an important role in determining the strength of composites in the case of inclusions (tetrahedrons and CNT bundles). In Ref. [10], MD simulations were also performed in order to investigate the effect of Ni coating on the mechanical behavior of single-walled CNTs and aluminum matrix composites. Their molecular dynamics simulation results show that the Young's modulus of the Ni coated CNT is much lower than the Young's modulus of the uncoated CNT, but the opposite result is obtained when the CNT is combined with aluminum. There are also many computational studies using the MD simulation to determine material properties in nano scales.

In the present study, MD simulations are used to study the effect of the alignments of CNTs in CNT-Al composite. During manufacturing CNT-Al composite, often it is assumed that CNTs are aligned parallel to each other. However, real CNT dispersion experiments are not ideal and they are inclined. Therefore it is crucial to investigate the effect of the alignments of CNT-Al composite. With MD simulations, the effects of the CNTs alignments and their sizes are investigated. For this, the relative angles of CNTs inside Al composite are varied and the stress and the strain curves are computed.

2. Molecular dynamic simulation

2.1 MD simulation condition

To study the effect of the alignment of CNTs inside Al block, the molecular dynamic simulation model shown in Fig. 1 is considered with LAMMPS. The brick Al matrix with $100\ \text{Å} \times 100\ \text{Å} \times 100\ \text{Å}$ is placed with the periodic boundary condition and a single CNT with an armchair (6,6) configuration is inserted in the z-direction at the center of the brick Al matrix. The radius of CNT is 4.03 Å and the average distance between the CNT and the Al atom is set to 7 Å. The AIREBO (adaptive intermolecular reactive empirical bond order) potential is used to simulate the atomic forces among carbon atoms. The EAM (embedded-atom method) potential which is known to be effective in modeling metallic atoms is applied to simulate the forces among Al-Al atomics. Then the numbers of C and Al atoms are 936 and 57916, respectively. At the interface between Al and C, the van der Waals dispersion forces with the Lennard-Jones (LJ) 12-6 potential are applied. The LJ potential in Eq. (1) is formulated as follows:

$$V_{\text{LJ}} = 4\varepsilon\left[\left(\frac{\sigma}{r}\right)^{12} - \left(\frac{\sigma}{r}\right)^{6}\right] \tag{1}$$

where the depth of the potential well is ε. The finite distance

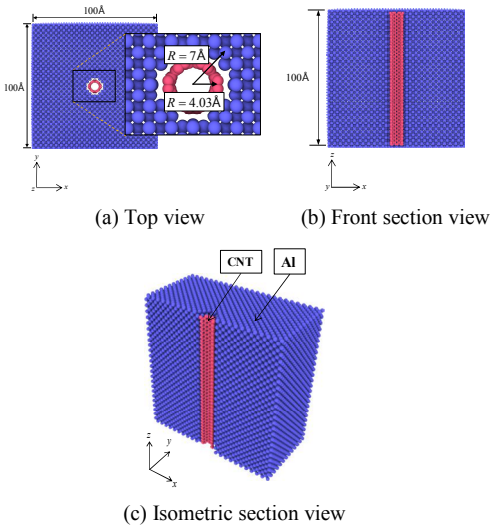

(a) Top view (b) Front section view

(c) Isometric section view

Fig. 1. The schematic representation of CNT-Al composites: (a) Top view; (b) front section view; (c) isometric section view.

at which the inter-particle potential is zero and the distance between atoms are denoted by σ and r, respectively. Among the Al atoms and the C atoms, the values associated to the LJ potentials in Eq. (1) are set as follows:

LJ potential among C atoms: $\varepsilon_C = 0.00296\,\text{eV}$ and $\sigma_C = 3.407$ Å. (2a)

LJ potential among Al atoms: $\varepsilon_{Al} = 0.41570\,\text{eV}$ and $\sigma_{Al} = 2.620$ Å. (2b)

LJ potential at the interface between Al-C atoms: $\varepsilon_{Al} = 0.035078\,\text{eV}$ and $\sigma_{C-Al} = 3.0135$Å. (2c)

The parameters in Eqs. (2a) and (2b) are obtained by the researches [15, 16]. The parameters along the interface are obtained by the geometric average, $\varepsilon_{C-Al} = \sqrt{\varepsilon_C \varepsilon_{Al}}$, and the algebraic average, $\sigma_{C-Al} = (\sigma_C + \sigma_{Al})/2$, respectively.

Among Al atoms, the EAM/alloy (embedded-atom method) potential is also applied.

$$V_i = F_\alpha\left(\sum_{i\neq j}\rho_\beta(r_{ij})\right) + \frac{1}{2}\varepsilon\sum_{i\neq j}\phi_{\alpha\beta}(r_{ij}) \tag{3}$$

where a pair-wise potential function is denoted by $\phi_{\alpha\beta}$ and the contribution to the electron charge density from the atom j of type β at the location of the i-th atom is ρ_β. The embedding function representing the energy required to place the i-th atom of the type α into the electro cloud. From a relevant research, it was reported that this EAM/alloy potential is appropriate for the MD simulation for Al atoms. In the present analysis, the EAM/alloy parameters for aluminum presented by Winey-Kubota-Gupta are used [24].

For a system of carbon atoms, the AIREBO (adaptive intermolecular reactive empirical bond order) potential in Eq. (4) is applied as follows:

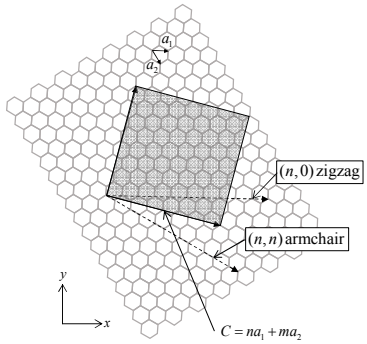

Fig. 2. CNT chiral vector.

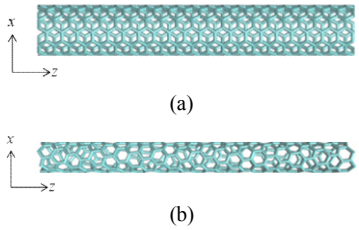

Fig. 3. (a) Structure of armchair CNT; (b) zigzag shape CNT.

$$V_i = \frac{1}{2}\sum_i \sum_{j\neq i}\left[V_{ij}^{REBO} + V_{ij}^{LJ} + \sum_{k\neq i,j}\sum_{l\neq i,j,k} V_{kijl}^{TORSION}\right]. \quad (4)$$

For CNT, the chiral vector in Fig. 2 is used and the diameter of CNT is computed by Eq. (5).

$$d = \frac{a}{\pi}\sqrt{(n^2 + nm + m^2)} = \frac{a}{\pi}\sqrt{3}n = 0.1356n \text{ nm}, (m = n,\ a = 0.246 \text{ nm}) \quad (5)$$

d : Diameter of carbon nanotube

a : The sizes of a_1 and a_2 .

Depending on the direction of the chiral vector, Armchair CNT and zigzag CNT can be constructed in Fig. 3. In the present study, the Armchair CNTs are inserted in Al composite.

3. Molecular dynamic simulation

3.1 Tensile simulation with a vertically aligned carbon nanotube

For the first MD analysis, the unit CNT-Al composite cell with the vertically aligned CNT is extended and Fig. 4 shows the snapshots during the simulation. The system is relaxed during 10 picoseconds with a timestep of 0.5 femtoseconds (NVT canonical ensemble for equilibrium, NVT or NPT for incremental analysis). In Figs. 4(b) and (c), the unit cell is extended uniformly, and no ruptures and dislocations is observed. With the extension in Fig. 4(d) with 11.25 Å, the slip band phenomenon is observed at the side of the unit cell. By

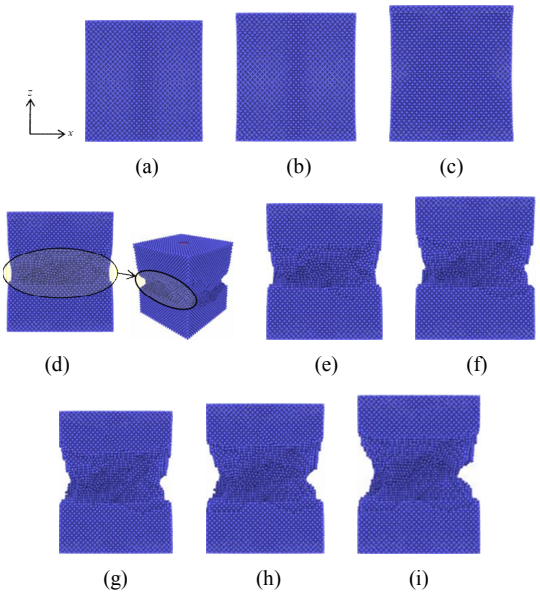

Fig. 4. Snap shots of CNT-Al composite material after initial stain u : (a) ($u = 0$ Å) ; (b) ($u = 3.75$ Å) ; (c) ($u = 7.5$ Å) ; (d) ($u = 11.25$ Å) ; (e) ($u = 15$ Å) ; (f) ($u = 18.75$ Å) ; (g) ($u = 22.5$ Å) ; (h) ($u = 26.25$ Å) ; (i) ($u = 30$ Å) .

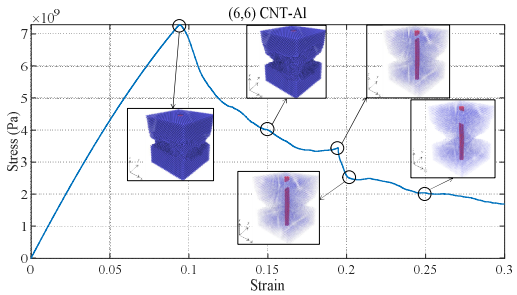

Fig. 5. The stress strain curve of CNT-Al composite ((6,6) CNT-Al).

increasing further in Figs. 4(e)-(i), the slips are propagated to the overall sides and the necking is observed.

Fig. 5 shows the stress-strain curve. The linear mechanical deformation is observed under 0.1 strain and the plastic deformation is observed. Due to the slip bands formation or the local buckling phenomena of the Al matrix or CNTs, the sudden drops in stress are observed. Around 0.18 for the strain, the CNT breaking phenomenon is observed. Due to the decrease bonding energy of the carbon atoms, the second sudden drop between 0.18 and 0.20 happens.

3.2 Tensile simulations with inclined carbon nanotube

As stated, in manufacturing the CNT-Al composite, it is hard to align carbon nanotubes inside aluminum composite and carbon nanotubes tend to be inclined. To simulate this situation, the molecular simulation models of the CNT-Al composite with the inclined CNT are considered (Fig. 6). The simple tensile simulations are conducted to obtain the stress-

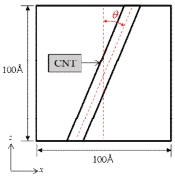

(a) Definition of CNT angle variation

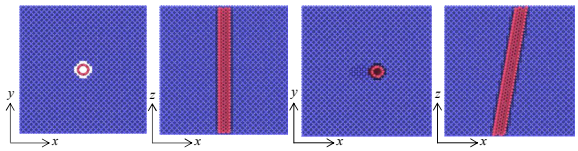

(b) $\theta = 0°$ (c) $\theta = 10°$

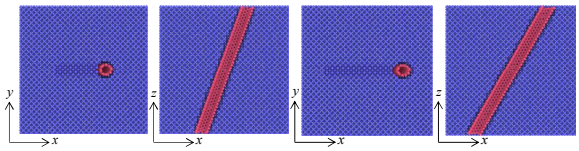

(d) $\theta = 20°$ (e) $\theta = 30°$

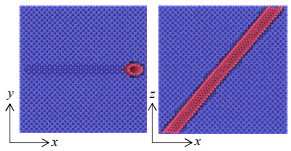

(f) $\theta = 40°$

Fig. 6. Sectional shapes of the Al-C composites with different inclined angles of carbon nanotubes: (a) Definition of CNT angle change; (b) $\theta = 0°$; (c) $\theta = 10°$; (d) $\theta = 20°$; (e) $\theta = 30°$; (f) $\theta = 40°$.

strain curves by varying the angle of carbon nanotubes. The atoms at the bottom surfaces ($z \in [0;5\ \text{Å}]$) are mechanically clamped and the atoms at the top surfaces ($z \in [95;100\ \text{Å}]$) are incrementally moved upward. Here the carbon atoms and the Al atoms at the top surface move.

Fig. 7 shows the stress-strain curves with 0, 10, 20, 30 and 40 inclined degrees between the carbon nanotube and aluminum composite. In the elastic region up to 0.05 strain, the stress-strain are almost same. The elastic Young's moduli are calculated approximately 86 GPa. However, when the CNTs are inclined, the ultimate strengths are decreased dramatically from 7.3 GPa to 4.3 GPa. Therefore, we can conclude that the orientation of CNT does not alter Young's modulus significantly but the ultimate strength is influenced a lot.

Table 1 summarizes the Young's modulus and the ultimate strength with the inclined CNTs. After the slip band phenomena, the overall stress-strain curves are similar to each other. However, it is observed that the mechanical resistances with the inclined CNTs are larger. Between 0.13 and 0.21 strain in Fig. 7(b), there are some drops due to the reduced bond energy of the carbon atoms and the weakened bonding energy.

Fig. 8 shows the ultimate strength curves of (6,6) CNT angle varying 0 to 40 inclined degrees between the carbon nanotube and aluminum composite. It is interesting that the deteriorations in the ultimate strengths with the inclined CNTs.

Table 1. The elastic modulus, the ultimate strength and ultimate strain according to the CNT angle change of the (6,6) CNT-Al composite.

	Ultimate strength (GPa)	Strain at ultimate	Young's modulus (GPa)
0°	7.3	0.094	91.84
10°	6.7	0.085	91.30
20°	6.2	0.078	90.24
30°	5.8	0.074	88.74
40°	4.3	0.055	86.62

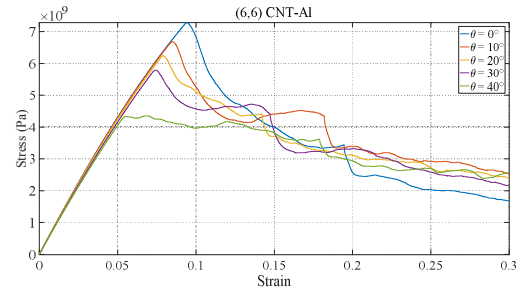

(a)

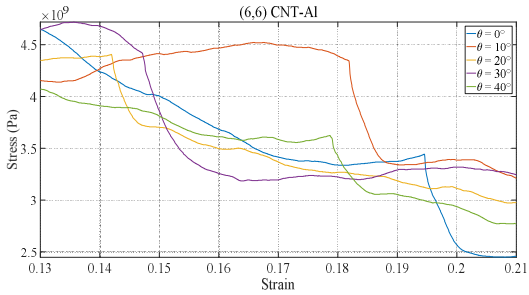

(b)

Fig. 7. (a) The curve of variation of axial stress with the axial strain according to CNT angle change ((6,6) CNT-Al); (b) the curve of variation of axial stress σ with the axial strain ε at 0.13 to 0.21.

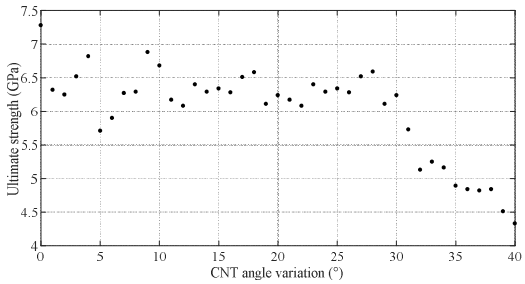

Fig. 8. Ultimate strength according to the CNT angle variation from 0 to 40 degrees.

3.3 The effect of CNT size and tilt angle on Young's modulus

The effect of the CNT size is studied by changing the Chiral vector shown in Figs. 9 and 10. The effects of the CNT size on

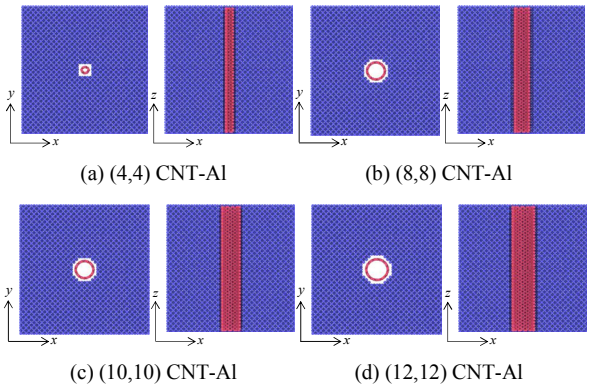

Fig. 9. Cross sections of CNT-Al composites with various chiral vectors.

mechanical strength were studied in Figs. 9 and 10. By increasing the CNT chiral vector inside Aluminum, the results in Fig. 10 show the increase of the ultimate strengths however, the buckling strains become lower or the CNT-Al composite becomes brittle. Fig. 11 shows the curves of Young's modulus with respect to the incline angles and the enlarged CNTs. By increasing the inclined angle, the Young's moduli of the composites are decreased. This can be interpreted as the lower strength of the inclined CNTs for axial load. By increasing the diameter of CNT, in Fig. 11 the overall Young's modulus is increased because the volume ratio of CNT to Al is increased. There are remarkable deteriorations for Young's modulus. From a quality engineering point of view, these deteriorations can be problematic. However, the modulus of elasticity is still higher than pure aluminum. In addition, the effect of the CNT on the diameter of the CNT was negligible when the CNT was tilted, and it was interesting that the CNT size had no effect on the Young's modulus for tilt angle above 40 degrees. These characteristics are difficult to be observed by nanoscale experiment.

The Young's moduli of a pure Al matrix and (6,6) Armchair CNT are set as $E_{\mathrm{Al}} = 82.2$ GPa and $E_{\mathrm{CNT}} = 771$ GPa, respectively. To predict the Young's modulus of the CNT-Al composite, the following mixing rule was proposed in Ref. [18]. The computed Young's moduli is about 0.06 GPa difference from the value in (6,6) CNT-Al Composites of Fig. 11.

$$E_{\text{Al-CNT}} = E_{\mathrm{Al}}V_{\mathrm{Al}} + E_{\mathrm{CNT}}V_{\mathrm{CNT}} = 93.2 \text{ GPa} \tag{6}$$

where the volume fractions of CNT and Al are $V_{\mathrm{CNT}} = 1.6$ % and $V_{\mathrm{Al}} = 98.4$ %, respectively. To predict the tensile strength of the aluminum matrix with inclined CNT, some methods such as micro-mechanics models, thermal expansion coefficient models, and fiber closure approximation models predicting the effect of the fiber orientation can be used. Micromechanics models are the models predicting the elastic properties of short-fiber reinforced composites from the knowledge of the matrix and the fiber elastic properties, fiber content, and fiber aspect ratio. The present study employs the Halpin-Tsai

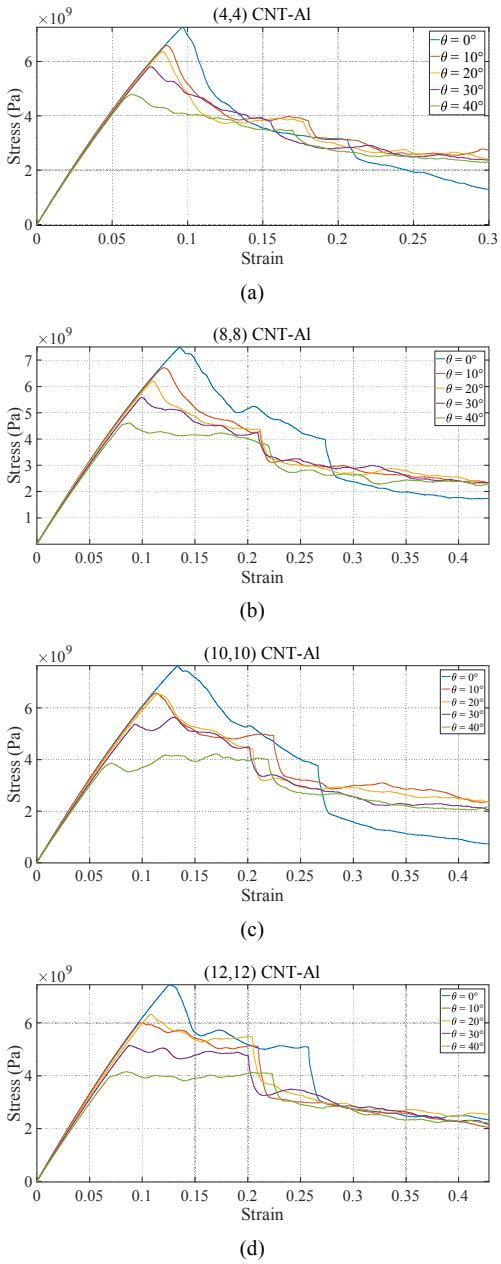

Fig. 10. The curve of variation of axial stress with the axial strain according to CNT chiral vector change: (a) (4,4) CNT-Al; (b) (8,8) CNT-Al; (c) (10,10) CNT-Al; (d) (12,12) CNT-Al.

equation and the Krenchel equation with the rule of the mixture method to predict the tensile strength of CNT-Al composite according to the CNT angle variation.

$$E_{\text{Al-CNT}} = E_{\mathrm{Al}}V_{\mathrm{Al}} + \eta_L \eta_0 E_{\mathrm{CNT}}V_{\mathrm{CNT}} \tag{7}$$

$$\eta_0 = \sum_n a_{fn}\cos^4\theta_n \Big/ \sum_n a_{fn}, \text{ where } \sum_n a_{fn} = 1. \tag{8}$$

In Eq. (7), the fibre-length correction factor η_L is set to $1/\cos(\theta)$ as the CNT increases its length by a factor of

Table 2. The elastic modulus, the ultimate strength and ultimate strain according to the CNT angle change of the (6,6) CNT-Al composite.

	Ultimate strength (GPa)	Strain at ultimate	Young's modulus (GPa)	Elongation at CNT local buckling point
(4,4) CNT-Al	7.26	0.09	89.96	0.21
(6,6) CNT-Al	7.30	0.09	91.84	0.20
(8,8) CNT-Al	7.50	0.09	93.45	0.19
(10,10) CNT-Al	7.62	0.09	95.88	0.19
(12,12) CNT-Al	7.44	0.09	98.41	0.18

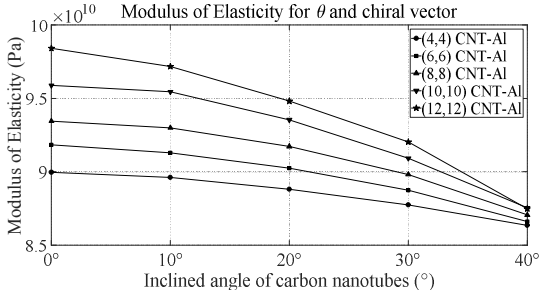

Fig. 11. Comparison of Young's modulus according to CNT inclined angle of carbon nanotube (0°~40°) and (4,4) ~ (12,12) CNT-Al.

$1/\cos(\theta)$ and the ratio between the cross-sectional area is denoted by a_{fn}. The Krenchel orientation efficiency factor η_0 is the ratio of the cross-sectional area of the fiber aligned at a constant angle to the applied load direction and the total area of the fiber to the cross-sectional area of the composite. Considering the angle change of CNT inside the CNT-Al composite, the Krenchel equation can be modified as follows:

$$\eta_0 = \cos^4\theta \tag{9}$$

$$E_{\text{Al-CNT}} = E_{\text{Al}}V_{\text{Al}} + E_{\text{CNT}}V_{\text{CNT}}\cos^3\theta\,. \tag{10}$$

Fig. 12 and Table 2 show the comparisons of the elastic modulus values between the MD simulation results and the modified rule of mixture (MROM) for (6,6) CNT-Al and (12,12) CNT-Al. As shown, the MROM theory agrees well with the simulation results. This implies that 1) the present MD simulation is properly modeling the behavior the CNT-Al composite and 2) the post buckling pheneomena and the detail behaviors inside the CNT-Al composite can be observed by the MD simulation. We can also conclude that the bulk model fits well at the nanoscale.

Comparing the modulus of elasticity of MD simulation results and the MROM results for each chiral vector, (6,6) CNT-Al shows differences less than 0.43 GPa. In the case of (12,12) CNT-Al, the differences are less than 0.97 GPa.

Table 3. The comparison of the Young's modulus between simulation results and the MROM results in (6,6) CNT-Al composites.

	MD (6,6) CNT-Al (GPa)	MROM (GPa)	Difference (GPa)
0°	93.28	93.22	0.06
10°	92.68	92.67	0.01
20°	91.33	91.12	0.21
30°	89.33	88.90	0.43
40°	86.51	86.43	0.08

Table 4. The comparison of the Young's modulus between simulation results and the MROM results in (12,12) CNT-Al composites.

	MD (12,12) CNT-Al (GPa)	MROM (GPa)	Difference (GPa)
0°	98.41	98.40	0.01
10°	97.18	97.50	0.32
20°	94.81	94.97	0.16
30°	92.02	91.35	0.97
40°	87.47	87.32	0.15

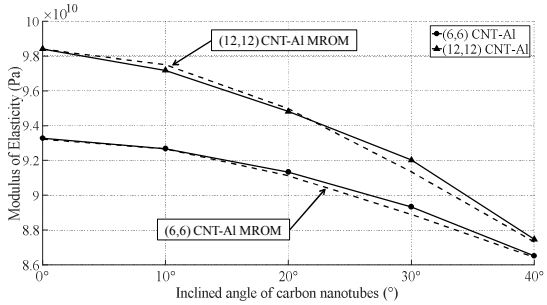

Fig. 12. Comparison of elastic modulus of simulation results and the MORM results.

3.4 Tensile simulations in x and y direction

Next, we studied the mechanical behavior of the composite when the load is applied in the x and y directions. For the completeness, Fig. 13 shows the estimated Young's modulus from the MD simulation results when the x and y direction loads are applied to the CNT-Al composites. Here the small differences can be observed in the Young's modulus. The Young's modulus of the CNT-Al composite is increased by about 0.2 GPa when the angle of CNT is increased by 20 degrees, but it decreases slightly at 30 degrees and then increases again in Fig. 13(b). Also the Young's modulus is increased by about 0.1 GPa when the angle of CNT is increased by 10 degrees, but it decreases slightly at 30 degrees and then increased again in Fig. 13(d). In Figs. 13(a) and (c), the plastic deformation of the aluminum matrix occurs, but no buckling phenomenon or breakage phenomenon of the CNT was ob-

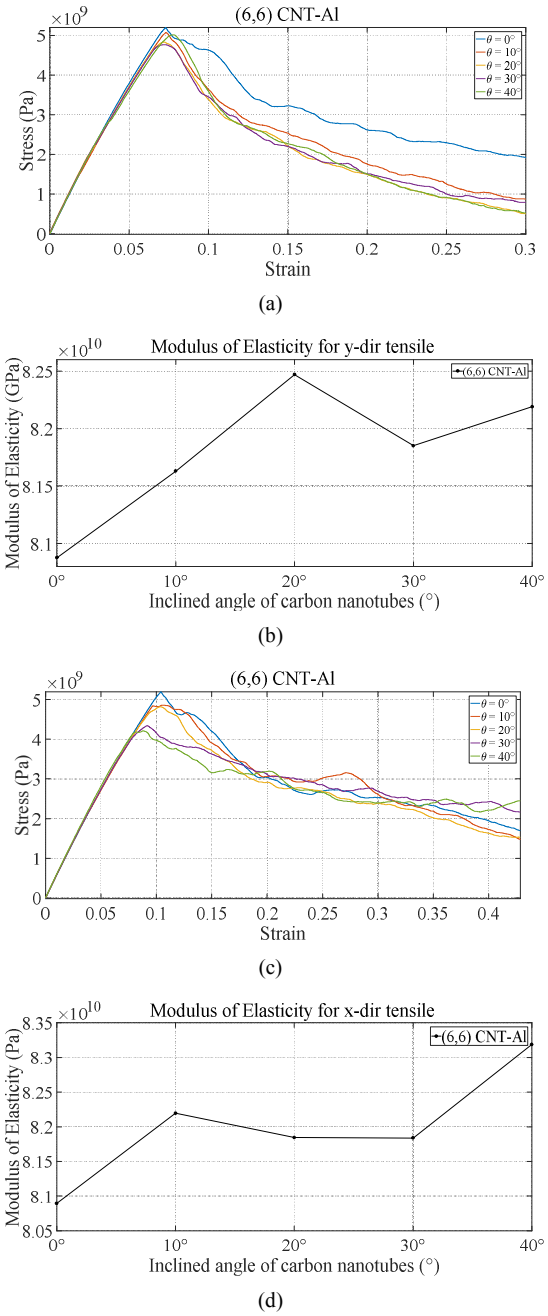

Fig. 13. The curve of variation of axial stress σ with the axial strain ε in the horizontal direction: (a) The stress-strain curve in the axial direction; (b) the elastic modulus of the carbon nanotube angle change; (c) the stress-strain curve in the transverse direction; (d) the elastic modulus of the carbon nanotube angle change.

served. This is because the stiffness of the CNT is stronger in the radial direction than in the longitudinal direction.

4. Conclusion

The purpose of this paper is to analyze the tensile behavior of CNT-Al composites using MD simulations. Mechanical properties were calculated by changing the geometric configuration of CNT. In addition, we confirm that the theory of the directionality of the fiber inside the matrix match the simulation results, indicating it can predict well the mechanical properties of nano-composite materials. The conclusions are summarized as followings.

(1) The CNT-Al composites (Chiral vector (6,6), 0 degrees) shows that Al slip band phenomenon can be observed at strain 0.1 and CNT breaking phenomenon at strain 0.18.

(2) As result of the mechanical properties of CNTs tilted at a certain angle, almost the same stress-strain curve was obtained in all cases in the elastic region up to 0.05. The modulus of elasticity of the composite is approximately 86 GPa. With the inclined CNTs, the strength of CNT-Al composites dramatically decreases from 7.3 GPa to 4.3 GPa. The size of the CNT does not significantly affect the modulus of elasticity but the yield strength of CNT-Al composites can be influenced.

(3) The tensile behavior of CNT-Al composites in various chiral vectors is simulated. As increasing the chiral vector of CNT, the bulk ratio of CNT to Al is also increased. The total Young's modulus increases accordingly and the composite becomes brittle. From the viewpoint of quality engineering, the brittle nature of the material can be problematic. Therefore, the volume ratio of the base material and reinforcement should be considered to be an important factor in reconstructing the composite material.

(4) The stress-strain curves and the elastic moduli by changing the CNT angle when uniaxially stretched in the horizontal direction are simulated. In x and y directions, the plastic deformation of the aluminum matrix occurs, but no buckling phenomenon or breakage phenomenon of the CNT was observed.

(5) Finally, the simple rule of mixture is modified by incorporating the Krenchel orientation efficiency factor and the fiber length correction factor and the theoretical Young's modulus is calculated and the results are compared with the simulation results.

Table 5. Ultimate strength for uniaxial tensile simulation in horizontal direction.

	X-dir tensile		Y-dir tensile	
	Ultimate strength (GPa)	Strain	Ultimate strength (GPa)	Strain
0°	5.19	0.07	5.19	0.07
10°	4.86	0.07	5.02	0.08
20°	4.82	0.07	4.83	0.07
30°	4.34	0.06	4.76	0.07
40°	4.18	0.05	5.02	0.07

Acknowledgments

This work was supported by the National ResearchFoundation of Korea (NRF) Grant [No: 2014M3A6B3063711(Global Frontier R&DProgram on Center for Wave Energy Control

based on Metamaterials)] funded bythe Korean Ministry of Science, ICT and Future Planning (MSIP) and was upported by the National Research Foundation of Korea (NRF) grant funded by the Korea government (MSIT) (No. 2018R1A5 A7025522).

Nomenclature

Å	: Angstrom
ε	: Potential well
σ	: The finite distance at which the inter-particle potential is zero
r	: The finite distance between atoms at which the inter-particle potential is zero
$\phi_{\alpha\beta}$	: Pair-wise potential function
ρ	: The electron charge density from the atom
α	: Electro cloud
d	: Diameter of carbon nanotube
a	: The size of chiral vector
u	: Engineering strain
E_{Al}	: The Young's moduli of a pure Al matrix
E_{Al}	: The Young's moduli of a pure Al matrix
V_{Al}	: The volume fractions of Al
V_{CNT}	: The volume fractions of Armchair CNT
η_L	: Fibre length correlation factor of CNT-Al composites
η_0	: The Krenchel orientation efficiency factor of CNT-Al composites
a_{fn}	: The ratio between the cross-sectional area of CNT-Al composites

References

[1] B. J. Carey, J. T. Tzeng and S. Karna, *Carbon nanotube aluminum matrix composites*, Army Research Lab Aberdeen Proving Ground Md (2010).

[2] H. Choi, J. Shin and D. Bae, The effect of milling conditions on microstructures and mechanical properties of Al/MWCNT composites, *Composites Part A: Applied Science and Manufacturing*, 43 (2012) 1061-1072.

[3] H. Choi, L. Wang, D. Cheon and W. Lee, Preparation by mechanical alloying of Al powders with single-, double-, and multi-walled carbon nanotubes for carbon/metal nanocomposites, *Composites Science and Technology*, 74 (2013) 91-98.

[4] C. Deng, D. Wang, X. Zhang and A. Li, Processing and properties of carbon nanotubes reinforced aluminum composites, *Materials Science and Engineering: A*, 444 (2007) 138-145.

[5] H. Kurita, H. Kwon, M. Estili and A. Kawasaki, Multi-walled carbon nanotube-aluminum matrix composites prepared by combination of hetero-agglomeration method, spark plasma sintering and hot extrusion, *Materials Transactions*, 52 (2011) 1960-1965.

[6] H. Kwon and M. Leparoux, Hot extruded carbon nanotube reinforced aluminum matrix composite materials, *Nanotechnology*, 23 (2012) 415701.

[7] T. Laha, Y. Chen, D. Lahiri and A. Agarwal, Tensile properties of carbon nanotube reinforced aluminum nanocomposite fabricated by plasma spray forming, *Composites Part A: Applied Science and Manufacturing*, 40 (2009) 589-594.

[8] W. Lee, S. Jang, M. J. Kim and J.-M. Myoung, Interfacial interactions and dispersion relations in carbon–aluminium nanocomposite systems, *Nanotechnology*, 19 (2008) 285701.

[9] M. Majid, G. Majzoobi, G. A. Noozad, A. Reihani, S. Mortazavi and M. Gorji, Fabrication and mechanical properties of MWCNTs-reinforced aluminum composites by hot extrusion, *Rare Metals*, 31 (2012) 372-378.

[10] H.-Y. Song and X.-W. Zha, Influence of nickel coating on the interfacial bonding characteristics of carbon nanotube–aluminum composites, *Computational Materials Science*, 49 (2010) 899-903.

[11] J. Stein, B. Lenczowski, N. Fréty and E. Anglaret, Mechanical reinforcement of a high-performance aluminium alloy AA5083 with homogeneously dispersed multi-walled carbon nanotubes, *Carbon*, 50 (2012) 2264-2272.

[12] T. Tokunaga, K. Kaneko and Z. Horita, Production of aluminum-matrix carbon nanotube composite using high pressure torsion, *Materials Science and Engineering: A*, 490 (2008) 300-304.

[13] S. Xiao and W. Hou, Studies of nanotube-based aluminum composites using the bridging domain coupling method, *International Journal for Multiscale Computational Engineering*, 5 (2007).

[14] Z. Hu, J. Zhang, Y. Yan, J. Yan and T. Sun, Molecular dynamics simulation of tensile behavior of diffusion bonded Ni/Al nanowires, *Journal of Mechanical Science and Technology*, 27 (2013) 43-46.

[15] A. Kutana and K. Giapis, Transient deformation regime in bending of single-walled carbon nanotubes, *Physical Review Letters*, 97 (2006) 245501.

[16] J. Munilla, M. Castro and A. Carnicero, Surface effects in atomistic mechanical simulations of Al nanocrystals, *Physical Review B*, 80 (2009) 024109.

[17] M. Shazed, A. Suraya, S. Rahmanian and M. M. Salleh, Effect of fibre coating and geometry on the tensile properties of hybrid carbon nanotube coated carbon fibre reinforced composite, *Materials & Design* (1980-2015), 54 (2014) 660-669.

[18] N. Silvestre, B. Faria and J. N. C. Lopes, Compressive behavior of CNT-reinforced aluminum composites using molecular dynamics, *Composites Science and Technology*, 90 (2014) 16-24.

[19] S. Simões, F. Viana, M. A. Reis and M. F. Vieira, Influence of dispersion/mixture time on mechanical properties of Al–CNTs nanocomposites, *Composite Structures*, 126 (2015) 114-122.

[20] S. M. H. Farrash, M. Shariati and J. Rezaeepazhand, The effect of carbon nanotube dispersion on the dynamic characteristics of unidirectional hybrid composites: An experi-

mental approach, *Composites Part B: Engineering*, 122 (2017) 1-8.
[21] S.-E. Lee and S.-H. Park, Enhanced dispersion and material properties of multi-walled carbon nanotube composites through turbulent Taylor-Couette flow, *Composites Part A: Applied Science and Manufacturing*, 95 (2017) 118-124.
[22] J. Wang and D. Y. Pui, Dispersion and filtration of carbon nanotubes (CNTs) and measurement of nanoparticle agglomerates in diesel exhaust, *Chemical Engineering Science*, 85 (2013) 69-76.
[23] J.-Z. Liao, M.-J. Tan and I. Sridhar, Spark plasma sintered multi-wall carbon nanotube reinforced aluminum matrix composites, *Materials & Design*, 31 (2010) S96-S100.
[24] J. Winey, A. Kubota and Y. Gupta, A thermodynamic approach to determine accurate potentials for molecular dynamics simulations: Thermoelastic response of aluminum, *Modelling and Simulation in Materials Science and Engineering*, 17 (2009) 055004.

Dong Mun Park received his B.S. degree in mechanical engineering from Dongyang Mirae University in 2017. Mr. Park is currently an M.S. candidate at Department of Mechanical Convergence Engineering, Hanyang University, Seoul, Republic of Korea.

Jun Hwan Kim received his B.S. degree in mechanical engineering from Hanyang University in 2014. Mr. Kim is currently an Ph.D. candidate at Department of Mechanical Convergence Engineering, Hanyang University, Seoul, Republic of Korea.

Seung Jun Lee received his B.S. degree in naval architecture and ocean engineering from Seoul National University in 2000. And he received his M.S. degree and Ph.D. in mechanical engineering from University of Michigan in 2006 and 2011, respectively. Dr. Lee is currently an Assistant Professor at Department of Mechanical, Robotics, and Energy Engineering, Dongguk University, Seoul, Republic of Korea.

Gil Ho Yoon received his B.S. degree in mechanical and aerospace engineering from Seoul National University in 1998. And he received his M.S. degree and Ph.D. in mechanical and aerospace engineering from Seoul National University in 2000 and 2004, respectively. Dr. Yoon is currently a Professor at School of Mechanical Engineering, Hanyang University, Seoul, Republic of Korea.